Precursor-Driven Reconfiguration of Bulk and Interface Enhances the Solar-Driven Water-Splitting Performance of Carbon Nitride Photoanode

Peer-reviewed author version

KASA, Abraham; Arumugam, LS; Vanleenhove, A; Jose, Vishal; Conard, T; REIS SANTOS, Daniely; D'HAEN, Jan; Simbula, A; LUTSEN, Laurence; Durantini, JE; Gimenez, S; BRAMMERTZ, Guy; SHUKLA, Sudhanshu & VERMANG, Bart (2025)
Precursor-Driven Reconfiguration of Bulk and Interface Enhances the Solar-Driven Water-Splitting Performance of Carbon Nitride Photoanode. In: Nano letters, 25 (50) , p. 17332 -17340.

DOI: 10.1021/acs.nanolett.5c04295
Handle: http://hdl.handle.net/1942/48079

Precursor driven reconfiguration of bulk and interface enhances the solar-driven water splitting performance of carbon nitride photoanode

Abraham Kasa,[1,2,3] Lakshman Sundar Arumugam,[4] Anja Vanleenhove,[5] Vishal Jose,[1,2,3] Thierry Conard,[5] Daniely Santos,[1,2,3] Jan D'Haen,[1] Angelica Simbula,[6] Laurence Lutsen,[1] Javier E. Durantini,[4] Sixto Giménez,[4] Guy Brammertz,[1,2,3] Sudhanshu Shukla,[1,2,3]* Bart Vermang[1,2,3]*

[1]Hasselt University, Imo-imomec, Martelarenlaan 42, 3500 Hasselt, Belgium

[2] EnergyVille, Thor Park 8320, 3600 Genk, Belgium

[3]Imec, Imo-imomec, Thor Park 8320, 3600 Genk, Belgium

[4] Institute of Advanced Materials (INAM), Universitat Jaume I, Av. Vicente Sos Baynat s/n., 12006 Castellón, Spain

[5] Imec, 3001 Leuven, Belgium

[6] Dipartimento di Fisica, Università di Cagliari, Monserrato, 09042 Italy

*E-mail: Abraham.Solomon.Kasa@imec.be; sudhanshu.shukla@imec.be

Abstract

Carbon nitride (CN) has emerged as a promising metal-free semiconductor for photoelectrochemical (PEC) water-splitting applications. However, its practical implementation is hindered by low photoactivity compared to inorganic photoanodes. We report excellent photoactivity of modified CN photoanodes for PEC water oxidation. Incorporating powder precursors during the synthesis induces favorable morphological modifications, enhanced layer ordering, and charge transfer. The powder thiourea-assisted growth of CN boosted the photocurrent by almost threefold. This enhancement is attributed to suppressed carrier recombination and improved charge transfer, and the formation of CN and SnS_2 heterojunctions. The champion CN photoanode achieved an excellent charge extraction efficiency of up to 69% and a benchmark photocurrent density with and without a hole scavenger of about 2.7 and 2 mA cm^{-2} for water oxidation at 1.23 V versus RHE in neutral 0.1 M Na_2SO_4 solution, with onset potential of 0.32 V *vs.* RHE and external quantum yield value reaching 42% at 440 nm.

Carbon nitride (CN) has garnered significant attention over the past decade as a promising metal-free and environmentally friendly semiconductor for driving photoelectrochemical (PEC) reactions, owing to its elemental abundance (C and N), excellent chemical stability, band gap tunability, and suitable energy band-edge position, along with its compatibility with low-cost and eco-friendly manufacturing.[1-3] However, the progress of CN-based photoelectrodes remains limited due to low photocurrent compared to state-of-the-art materials.[4-8] The predominant inhibiting factors for photocurrent in CN photoelectrodes are rooted in its moderate light-harvesting properties, and poor charge transport due to low conductivity and high charge recombination rates. Moreover, the interface between CN and contact layers is also critical, especially for the sluggish oxidation reaction kinetics, where the build-up photogenerated charges decreases the photoconversion efficiency. Inadequate mechanical and electronic coupling to the conductive substrates results in weak adhesion and interfacial charge transfer barrier, further hindering its performance and large-scale adoption. These cumulative factors have stagnated the development of CN-based PEC cells.[9]

Synthesizing high-quality CN films with cohesive contact with conductive substrates is crucial for CN photoanode advancement. Previous efforts to address this relied on different preparation techniques such as thermal vapor condensation,[10-12] solvothermal methods,[13, 14] spin coating,[15, 16] doctor blading,[17, 18] microcontact printing,[19] co-condensation of CN monomers,[20] and sol-gel processing.[21] Among these, vapor-based deposition methods yield high-quality film on variety of substrates,[22] and direct growth of monomers on the conductive substrate, followed by calcination at high temperature, has demonstrated improved film adhesion and enhanced photocurrent density.[20, 23] This two-step approach provides a facile platform to obtain homogenous films with tailored structural, optical, electronic, and photochemical properties through rational synthesis, molecular functionalization, doping, and hetero-interface formation. For instance, nitrogen-rich organic compound, such as melamine, incorporation during the

thermal polymerization process enhances the electronic coupling with a conductive substrate and improve photocurrent.[20] Doping Na and B in the similar process extends visible light absorption up to 550 nm and increases the photocurrents.[24] Similarly, constructing dual-layer CN films from co-condensation of a supramolecular precursor on carbon source polymer matrix,[25] and directly employing a supramolecular complex[26] have also been reported to improve the film quality. Strikingly, some sulfur-containing precursors improve the interface by reinforcing the chemical adhesion of CN films to FTO substrates and promoting charge migration across the interface due to the adventitious heterojunction formation.[27] Despite significant progress in the fabrication of CN films, photocurrents from CN photoanodes have not exceeded few hundreds of microampere, reaching only up to 910 μA cm^{-2} at 1.23 V *vs*. RHE under one-sun illumination.[25] Such performance is notably lower compared to its theoretical limit and analogous metal oxide photoanodes such as Fe_2O_3, $BiVO_4$, TiO_2, and WO_3 for water oxidation.[28] For instance, $BiVO_4$ can deliver stable photocurrents of up to 6 mA cm^{-2} at 1.23 V *vs*. RHE under AM1.5G illumination.[29] Thus, development of viable methods that allow the formation of CN films with tailored structures with high performance remain a central issue to realize the practical implementation of CN photoanodes PEC cells.

Herein, we developed a precursor-guide in-situ growth method to synthesize nanoporous carbon nitride thin films to holistically improve performance *via* enhanced molecular-level linkages and structural ordering of layered CN sheets, nanoporous morphology, and better interfacial charge separation from heterojunction (Z-scheme) formation. The rich CN chemistry and precursor engineering allows direct regulation of the structure during the film growth and promotes interaction at molecular level, leading to enhanced optical absorption and reduced charge transfer resistance. The thermal decomposition of nitrogen (melamine, urea) and sulfur-rich (thiourea) supramolecular modifiers direct the growth and dictates the chemistry of the bulk as well as the back charge-selective interface. The optimized CN photoanode

achieved a remarkable improvement in the photocurrent density for water oxidation reaction, reaching up to 2.7 mA cm^{-2} (with H_2O_2 hole scavenger) and 2 mA cm^{-2} (without hole scavenger) at 1.23 V *vs*. RHE in 0.1 M Na_2SO_4 aqueous solution under standard AM1.5 one-sun illumination with low onset potential of 0.32 V *vs*. RHE, and a high charge transfer efficiency of up to 69%,. The modified CN photoanode demonstrated excellent PEC performance, advancing the potential of this material for practical applications in PEC systems.

In this study, CN thin films were deposited on fluorine-doped tin oxide (FTO)-coated glass using thiourea precursor, based on the method reported by Qin *et al*. in 2020[20] (see methods). The deposition of thiourea resulted in a uniform white layer on the FTO substrate upon drying (Fig.1a, see Fig.S1 and S2). Calcination of the film produced a nanostructured flake-like porous CN film on FTO (Fig.S3), with thickness optimized by controlling the initial layers of thiourea films (Fig.S4 and S5). The modification of the CN electrode was performed by calcination in the presence of melamine, urea, and thiourea monomers, referred as CN_M, CN_U, and CN_T, respectively. The SEM image shows the formation of island-like structures, indicating preferential polymerization growth process (Fig.S6). A study by Fung *et al*. elucidated the role of sulfur in the growth of CN films by preferential bonding with Sn. This interaction initializes the formation of CN and leads to polymerization cascades that form islands on the FTO substrate.[27]

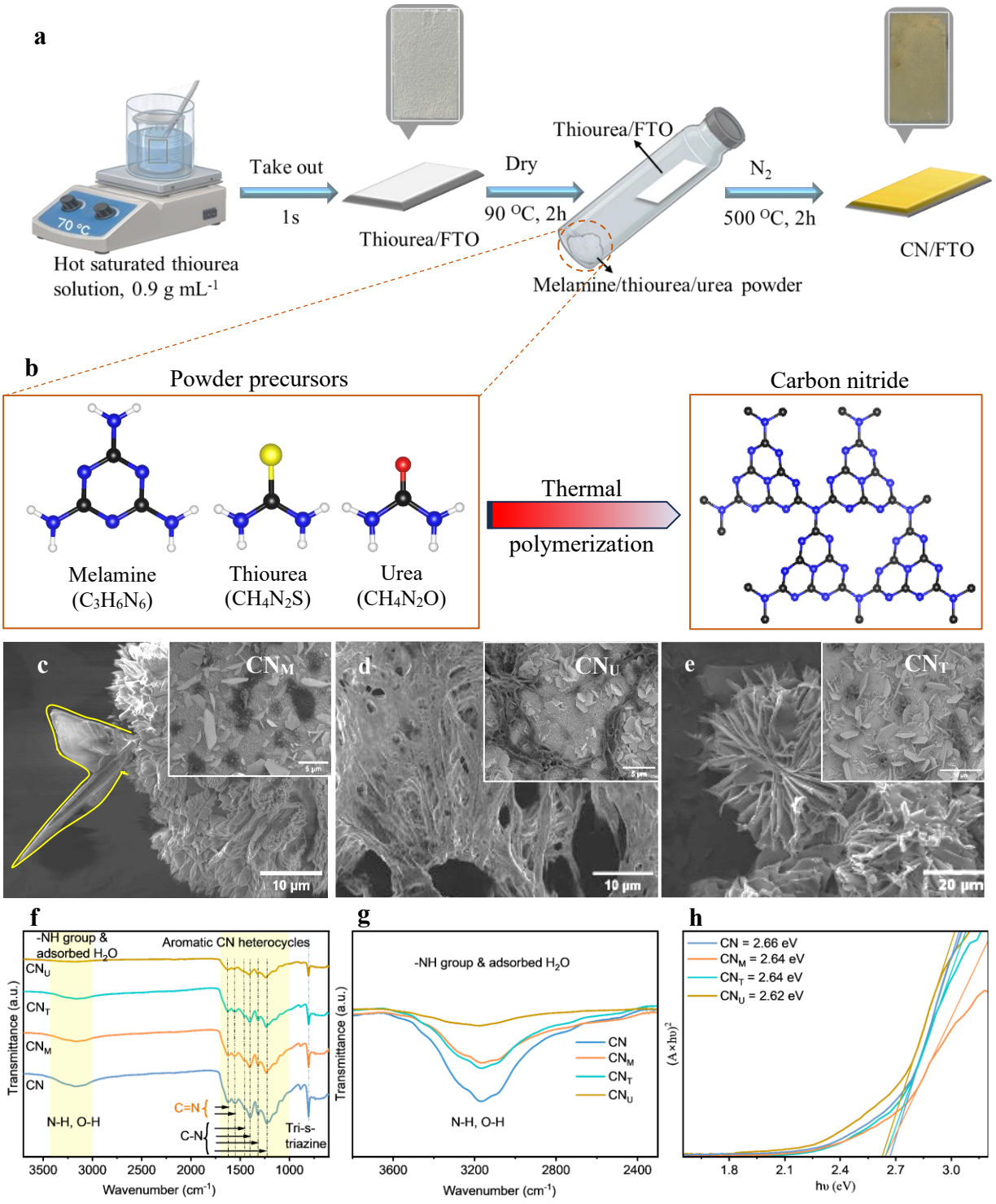

Figure 1: Synthesis of CN photoanode. a) Schematic representation of the synthesis of modified CN films. b) Molecular structure schematics: Atom's colour: black, blue, white, red, and yellow represent C, N, H, O, and S, respectively. SEM images of (c) CN_M, (d) CN_U, and (e) CN_T (Insets are the SEM images at higher magnifications). (f) FTIR spectra g) Expanded FTIR spectra in the range of 2300–3800 cm^{-1}. (h) Tauc plot analysis for direct transitions of CN electrodes.

Incorporation of melamine resulted in the formation of rod-like structures on the surface of CN, as highlighted in Fig.1c. The extent of these structures increased with the amount of melamine added during calcination (Fig.S7). The CN_U electrode (Fig.1d) shows a rod-like structure and a hexagonal sheet-like structure on the FTO. Similarly, the CN_T electrode (Fig.1e and Fig.S8a) shows flower-like porous nanosheet structures along with hexagonal structures. The carbon nitride covers the entire surface of FTO (Fig.S8b) in addition to forming an island structure. Complementary EDX analysis on flower-like islands structures predominantly show carbon (C) and nitrogen (N) atoms (Fig.S9a and b). In contrast, the hexagonal platelet structure shows Sn, S, C, N, and O (Fig.S10a and c) elements, indicating the possible heterostructure modification of CN.

The functional groups and chemical bonds of the synthesized electrodes were characterized using Fourier-transform infrared (FTIR) spectroscopy (Fig.1f). All the modified electrodes exhibited similar spectral patterns to the reference CN electrode. The strong peak at 806 cm^{-1} corresponds to the breathing mode and bending vibration of tri-*s*-triazine units, confirming the successful formation of CN. [30] The vibration bands within the 900 to 1750 cm^{-1} range correspond to the stretching modes of C-N heterocycles, including C=N stretching vibrations at 1543 and 1619 cm^{-1}, and aromatic C-N stretching vibrations at 1231, 1316, 1399, and 1451 cm^{-1}.[31, 32] In this region, CN_M, CN_T, and CN_U showed a slight blue shift compared to CN (Fig.S11), indicating shorter chemical bonds due to enhanced structure conjugation and polymerization from molecular modification.[33] The broad peak observed between 3000 and 3500 cm^{-1} is attributed to N-H and O-H stretching vibrations, originating from the -NH group of amino and adsorbed H_2O, respectively. [32, 34] The CN_U electrode showed a generally lower peak intensity, due to poor film formation and inadequate adhesion of the carbon nitride to the FTO. Furthermore, careful observation of the spectra of the CN_M, CN_T, and CN_U shows reduced intensities in the broad peaks between 3000 and 3500 cm^{-1} (Fig.1g). This reduction suggests

that incorporating powder precursors decreases the terminal amine groups, promoting the formation of ordered carbon nitride sheets.[35] UV-Vis spectroscopy of CN_M, CN_T, and CN_U showed direct transition characteristics with bandgap in the range of 2.66 to 2.62 eV (Fig.S12 and Fig.1h).

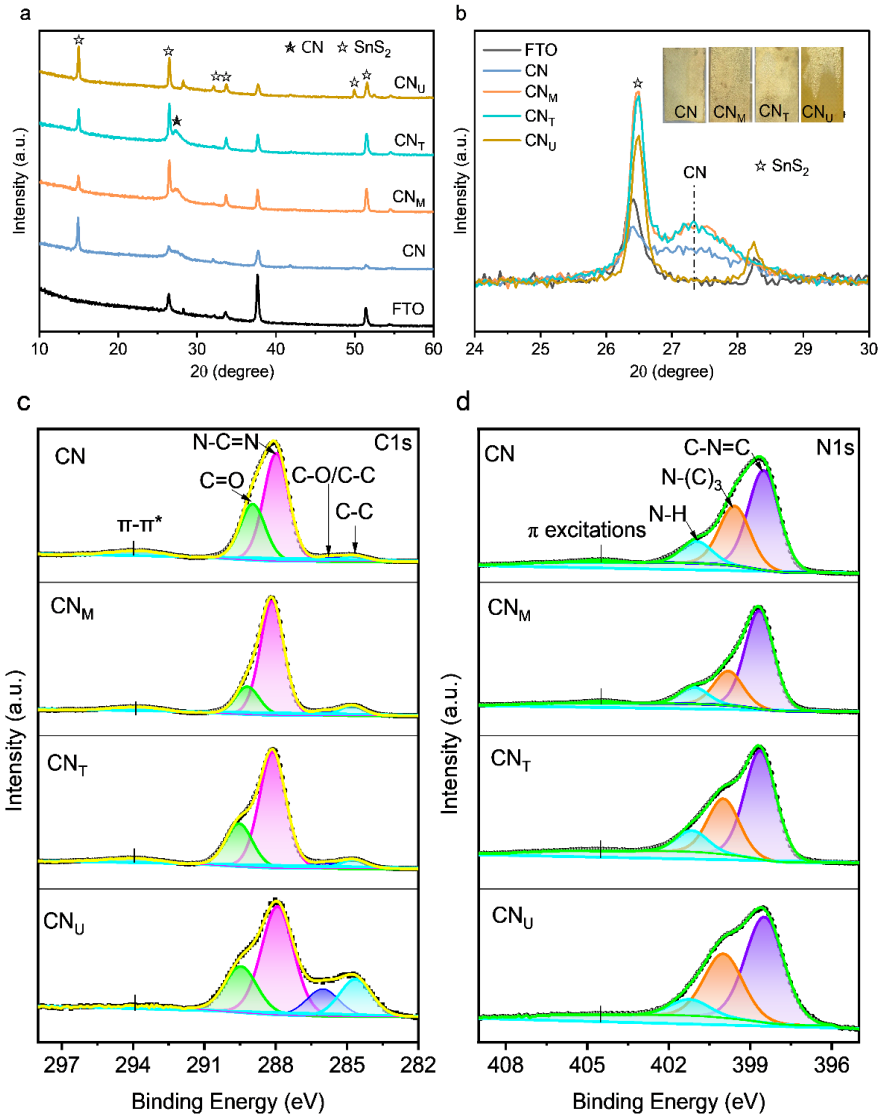

Figure 2 Characterizations of the electrodes: a) XRD patterns of modified CN films. b) XRD in the specific 2θ range of 24°-30° (inset: digital images of the films). High-resolution XPS spectra with deconvoluted peak fitting for (c) C 1s, (d) N 1s.

The X-ray diffraction (XRD) patterns (Fig.2a) show that the diffraction peak intensity at 27.5°, associated with the interlayer stacking of the aromatic system, slightly increases for CN_M and CN_T films compared to the reference CN film (Fig.2b). This enhancement suggests structural coherence within the (002) plane owing to enhanced crystallinity and a more uniform distribution of atoms. However, the CN_U electrode exhibited a very weak CN peak, due to poor film formation (Fig.2b-inset), consistent with FTIR analysis.

To further understand the effect of melamine, thiourea, and urea on the surface chemical composition and oxidation state of the electrodes, X-ray photoelectron spectroscopy (XPS) analysis was performed. The atomic concentrations of the electrodes were determined from the intensities of high-resolution XPS spectra. As shown in Table S1, the atomic concentrations of CN, CN_M, and CN_T are similar, with C and N detected as the main elements next to traces of S, Sn, and O, indicating that the addition of melamine and thiourea during calcination does not significantly affect the total atomic composition. Additionally, the calculated C:N ratio of the samples is also close to the theoretical value of 3:4 (Table S2). However, CN_U exhibits a notably higher O concentration, along with a significant amount of Sn and S, associated with the increased oxygen content from the urea precursor (Fig.S13a and Table S1). The high-resolution C 1s spectrum (Fig.2c) of CN reveals peaks at 284.6, 285.8, 287.0, and 289.0 eV, corresponding to adventitious carbon, partly oxidized carbon (C-O/adventitious carbon), sp^2-hybridized N–C=N coordination, and C=O groups, respectively. [36-38] Similar spectral features were observed for CN_M, CN_T, and CN_U, with slight shifts in binding energies. An increase in intensity of the N–C=N bonds was detected in the modified samples (Table S3), suggesting enhanced sp^2 bonding and a more ordered structure. This increased ordering enhances the interlayer stacking, consistent with the increased XRD peak (Fig.2b). In addition, a reduction in C=O peak intensity is observed for CN_M, CN_T, and CN_U, which may contribute to enhanced PEC performance.[39] The N 1s spectrum (Fig.2d) of CN displays three main peaks at 398.5, 399.6, and 401.0 eV,

corresponding to sp^2 C–N=C bonds, tertiary nitrogen N–$(C)_3$ groups, and amino groups (-N-H), respectively, [40] while, a peak at 404.6 eV is often attributed to charging effect or π-excitation.[41-43] Notably, slight shifts in the N 1s peaks are observed for the modified electrodes compared to CN. In addition, an increased ratio of C-N=C to -N-H species was observed for CN_M and CN_T compared to CN, providing further evidence of precursor-induced structural rearrangements (Table S4). The observed shifts in both C 1s and N 1s binding energies, along with the increased intensity of sp^2-bonded C and N within the triazine rings, further confirm interactions between the added powder precursors and C/N atoms. The high-resolution O1s spectra of CN, CN_M, and CN_T show a peak at 532.3 eV, associated with the C=O bond.[44] However, CN_U exhibited increased peak intensity and different peak shape, which is likely due to its higher oxygen content observed in elemental analysis and varying chemical environments and surface heterogeneity from the urea decomposition (Fig.S13b). The analysis of S 2p spectrum confirms S^{2-} species, S-C and S-O bonding signature (Fig.S13c).[45, 46] The Sn 3d spectrum (Fig.S13d) exhibits peaks at 486.7 and 495.1 eV, corresponding to Sn $3d_{5/2}$ and Sn $3d_{3/2}$, respectively, demonstrating the formation of Sn^{4+}.[47] These findings align with XRD results, confirming the formation of SnS_2. The Sn 3d and S 2p peaks in CN_M, CN_T, and CN_U show similar features with a slight shift to lower binding energies. Shifts in binding energy in XPS spectra are commonly attributed to two mechanisms: variations in the electronegativity of metal ions and strong interactions (electron transfer) between nanocrystals.[48-50] In this study, the calcination of the thiourea film resulted in the formation of an SnS_2 layer between the CN film and the FTO substrate. Further characterization and discussion of the exposed FTO forming SnS_2 is presented in the supplementary file (Fig.S14).

The photoelectrochemical (PEC) properties of the electrodes were measured using a three-electrode configuration in 0.1M Na_2SO_4 electrolyte under one-sun illumination. The electrodes prepared under different synthesis conditions exhibited varying photocurrent densities (Fig.3a). The linear sweep voltammetry (LSV) under both front and back illumination

revealed that back illumination resulted in higher current densities (Fig.S15a), suggesting electron-limited transport[51] and the potential for further optimization of the film thickness. However, increasing the thickness by adding more layers through the dip-dry cycle led to a decline in photocurrent (Fig.S15b), due to diffusion limitations and decreased conductivity [26]. The incorporation of powder precursors notably enhanced the overall PEC water oxidation performance (Fig.3a and Fig.S16). The electrodes prepared with 25 mg of powder precursors produced the highest photocurrent density. The LSV measurements (Fig.3b) showed a significant photocurrent increase from 0.5 mA cm^{-2} for CN to 0.56, 1.27, and 1.44 mA cm^{-2} at 1.23 V *vs.* RHE, for CN_M, CN_U, and CN_T, respectively. The CN_T electrode exhibited the highest photocurrent density with an onset potential of 0.36 V *vs.* RHE, and the photocurrent further increased at higher applied bias. The maximum applied bias photon-to-current conversion efficiency (ABPE) of CN_T is 0.11% at 1.09 V vs RHE, about four times as high as the maximum value of CN (0.03%) (Fig.3c). Electrochemical Impedance Spectroscopy (EIS) analysis (Fig.S17a) revealed that molecular precursor modification significantly improved the charge transfer characteristics of the CN electrodes. The Nyquist plot showed the smallest semicircle for CN_T, indicating better charge transfer. Thus, the structural and morphological modifications induced by the incorporation of thiourea precursors suppress the charge transfer resistance and carrier recombination and promote more efficient charge separation and migration.

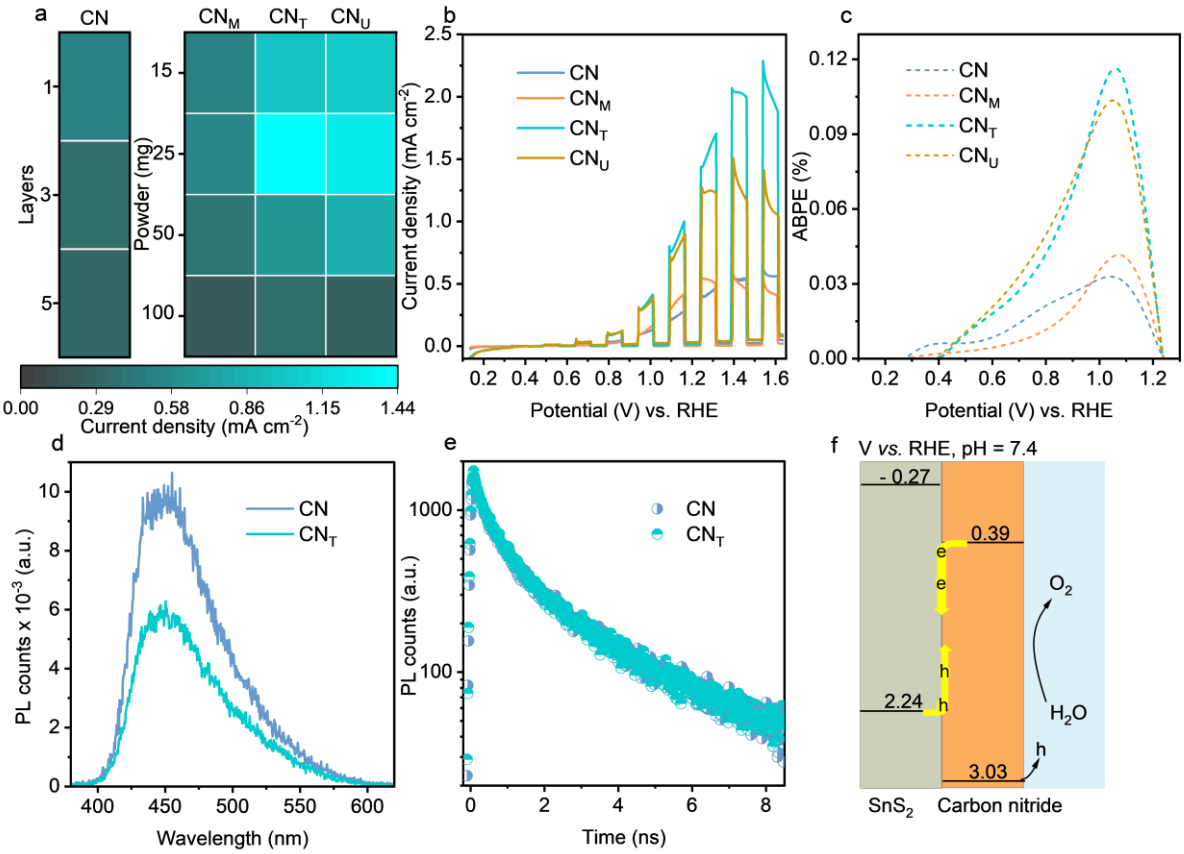

Figure 3: PEC performance characterization. a) Photocurrent density of carbon nitride photoanodes under varying synthesis conditions, including film thickness, powder precursors, and their amount, at 1.23 V *vs.* RHE under one-sun illumination in 0.1M Na_2SO_4 aqueous solution. b) LSV measurements under chopped 1-sun (back) illumination. c) ABPE analysis. d) steady-state PL, and e) time-resolved PL decay spectra. f) Energy level diagram of CN_T and exposed FTO relative to water redox reactions, determined using Mott-Schottky plots and optical bandgaps from Tauc plot analysis.

Mott-Schottky (MS) analysis of the CN_T electrode confirms its n-type semiconductor behavior (Fig.S17b) and is further used to determine the flat band potential (V_{fb}). For n-type semiconductors, the V_{fb} is inferred to be located near the conduction band (CB) edge.[52-54] Thus, the CB edge position of CN_T is estimated to be at 0.39 V vs. RHE, and based on its band gap, the valence band (VB) maximum is estimated to be at 3.03 V vs. RHE. To gain further insights into the charge separation mechanism in the CN_T electrode, the SnS_2 interface between the CN layer and the FTO substrate was analyzed after mechanically scratching the top CN film. From

MS analysis, the CB edge of SnS_2 is determined to be -0.27 V vs. RHE, while its band gap, as derived from Tauc plot analysis (Fig.S17c), is 2.51 eV, rendering its VB edge to be 2.24 V *vs*. RHE. While MS establishes the energy band positions, it does not reveal charge transfer directionality. Therefore, we conducted steady-state and transient photoluminescence analysis of the control (CN) and best (CN_T) to confirm charge transfer, as shown in Figure 3d and e. The PL quenching of the steady-state PL emission for CN_T indicates enhanced charge transfer of photoexcited carriers. Additionally, the time-resolved transient PL decay lifetimes show similar lifetimes for CN and CN_T, which is attributed to the bulk lifetime. Combined with the lower photocurrent observed for the interlayer SnS_2 (Fig.S17d), the result indicates a Z-scheme heterojunction configuration (Fig.3f), which facilitates the recombination of low-energy carriers at the back interface and enhances the charge transfer process.[55] Notably, the PL emission also extends to ~600 nm with a low-energy tail emission centered around 530 nm. Although favorable for light absorption, the origin of this extended tail remains unclear so far. The below bandgap tail emission appears, regardless of the 1- or 2-photon excitation condition (2-photon excitation allows to probe deeper through the thick CN films, providing more in-depth information) (Fig.S17e). This suggests that the emission process is exploiting the same material with the similar nonlinear properties (for example, the same 2-photon absorption cross-section), and thus that the low energy emission most likely originates from the carbon nitride layer itself rather than a SnS_2 layer at the FTO/CN interface. We cautiously attribute the observed extended optical response to sub-bandgap electronic transition in carbon nitride[56].

The performance of the CN_T electrode was further optimized by lowering the concentration of the aqueous thiourea solution from 0.9 to 0.6 and 0.3 g mL^{-1}, labeled as $CN_{T0.6}$ and $CN_{T0.3,}$ respectively (Fig.S18). The reduced thickness is expected to allow greater light penetration and better charge transport. The LSV measurement of the electrodes (Fig.4a and Fig.S19) shows that $CN_{T0.6}$ generated the highest photocurrent of 2 mA cm^{-2} at 1.23 V *vs*. RHE.

In the presence of 0.5M H_2O_2 hole scavenger, photocurrent increased to 2.7 mA cm^{-2} due to efficient hole extraction efficiency (Fig.4b). The detailed characterization of $CN_{T0.6}$ (Fig. S20-S22) and the effect of $CN_{T0.6}$ calcination temperature and electrolyte conditions on the performance can be found in SI (Fig. S23-S25).

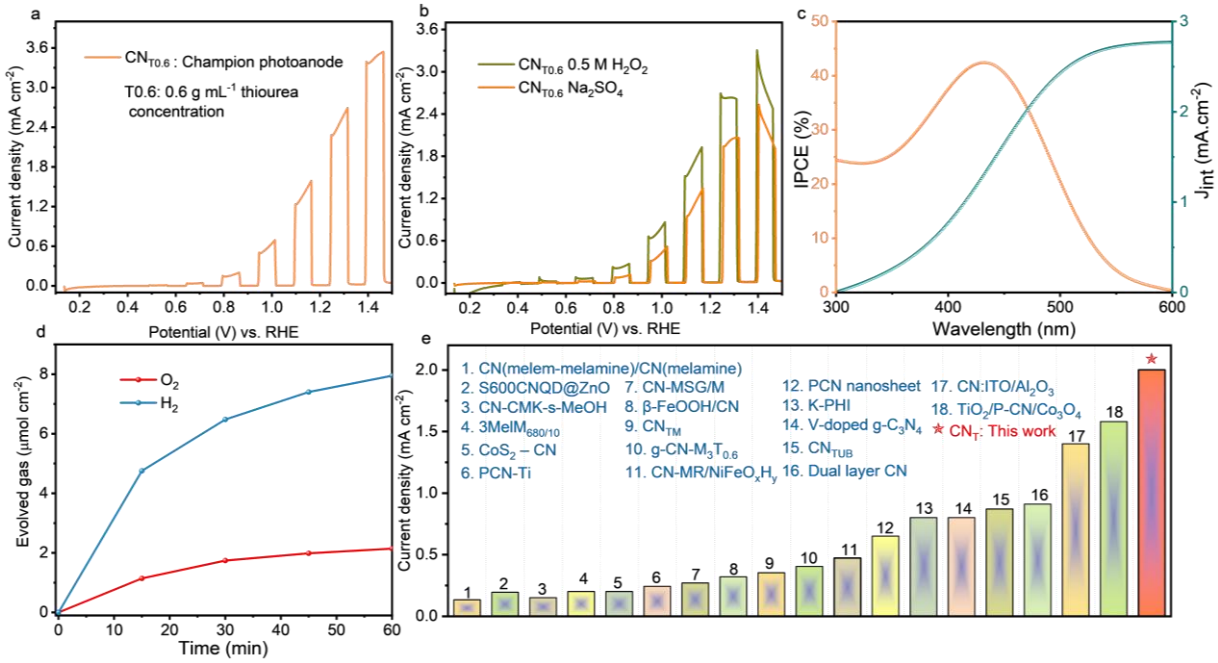

Figure 4 Characterization of optimized photoanodes. a) Photocurrent density of champion $CN_{T0.6}$ photoanode b) LSV measurements of $CN_{T0.6}$ in 0.1 M Na_2SO_4 with and without hole scavenger (0.5 M H_2O_2). c) IPCE measurement of $CN_{T0.6}$ photoanode at 1.23 V vs RHE and the integrated photocurrent density. d) Evolved O_2 and H_2 gases generated from the photoelectrochemical cell. e) Photocurrent density of carbon nitride-based photoanodes from recent reports (details available at Table S5).

The calculated charge transfer efficiency of the $CN_{T0.6}$ electrode is approximately 69% at 1.23 V *vs*. RHE (Fig.S26), which is notably high considering the absence of any cocatalyst. The enhanced charge separation is further evidenced by the lower onset potential (Fig.S27a) observed in the $CN_{T0.6}$ (0.32 V) compared to CN_T electrode (0.36 V *vs.* RHE). Furthermore, the $CN_{T0.6}$ demonstrated the highest APBE of 0.16% at 1.09 V *vs.* RHE (Fig.S27b) with smaller semicircle in the Nyquist plot, indicating a reduced charge transfer resistance (Fig. S27c).

The photoanodes demonstrated excellent reproducibility (Fig.S27d). Figure 4c shows the incident photon-to-current conversion efficiency (IPCE) of the $CN_{T0.6}$ electrode at 1.23 V *vs*. RHE in a 0.5M Na_2SO_4 electrolyte. The highest IPCE of ≈ 42% was achieved at around 440 nm, with photoresponse extended up to 600 nm, consistent with the absorption and PL observations. The integrated photocurrent density shows only slightly higher value (2.8 mA cm^{-2}) compared to those observed in the LSV measurements. The production of hydrogen (H_2) and oxygen (O_2) gases during the PEC experiment using the $CN_{T0.6}$ photoanode was measured at 1.23 V *vs.* RHE under 1-sun illumination (Fig.4d). Gas evolution rate of 7.95 and 2.14 μmol h^{-1} cm^{-2} H_2 and O_2 respectively. Despite high current density from the photoanode, the calculated Faradaic efficiencies (FE) for OER and HER were 12% and 44%, respectively. The low FE and the deviation from the expected stoichiometric ratio between O_2 and H_2 gas evolution are attributed to instability under prolonged irradiation (Fig.S28), which indicates that a significant portion of the measured photocurrent is not contributing to water oxidation but rather arises from layer degradation. The high photocurrent, therefore, primarily reflects the intrinsic photoactivity of the electrode rather than its water oxidation efficiency[57]. The slow kinetics in the absence of co-catalyst could drive self-oxidation of CN in the presence of four e^--h^+ pairs involved in water oxidation reaction. Additional losses stem from membrane-less device configuration, which allows mixing of the evolved hydrogen and oxygen gases, and parasitic reactions. Post-operation analysis does not show any notable changes in morphology or delamination (Fig.S29-S31), supporting the above-mentioned possibilities. Enhancing stability and improving the interfacial charge-transfer kinetics between the electrode and the electrolyte are crucial to increasing the FE.

To the best of our knowledge, the $CN_{T0.6}$ electrode generated the highest performance reported to date for carbon nitride photoanode in PEC water oxidation without a hole scavenger, as shown in Fig.4e. The superior water oxidation performance of $CN_{T0.6}$ can be attributed to: (i) an optimized film thickness, which minimizes the recombination of photogenerated charge

carriers, (ii) enhanced charge separation, as evidenced by a lower onset potential, and excellent transfer efficiency, and (iii) the formation of an Z-scheme heterojunction between the CN and SnS_2 layers, which further facilitates effective charge separation. However, addressing the operation instability is critical for ensuring long-term operation and deployment in practical solar-to-fuels farms.

This study presents a simple and facile synthesis method for carbon nitride photoanodes with excellent photocurrents for PEC water oxidation. Our work reveals the importance of rational precursor selection at the second polymerization step of the monomer, which has mostly relied on melamine. Introducing nitrogen-rich urea and sulfur-rich thiourea precursors at the second step showed marked improvement in the photoanode performance. Particularly, the co-polymerization of thiourea/FTO film with thiourea powders significantly enhances PEC water oxidation activity with photocurrent reaching above 2 mA cm^{-2} at 1.23 V *vs.* RHE, with a high charge extraction efficiency of up to 69% and extended photoresponse up to 600 nm, a benchmark for carbon nitride-based photoanode.

Supporting information

Materials, experimental methods, characterizations, PEC measurements, SEM images, EDX analysis, XRD patterns, UV-vis spectra, FTIR spectra, XPS data, LSV measurements, TRPL measurements, Mott-Schottky analysis, chronoamperometry measurements, electrochemical impedance spectroscopy, comparisons of the performances, comparison of the deconvoluted XPS peaks, digital images of the samples, and additional references.

Acknowledgements

S.S. acknowledge support from the European Union's Horizon Europe research and innovation programme *via* PHOENIX project (grant agreement No 101172764). S.S. and B.V. acknowledge KESPER (M-ERA.NET) and Interreg FOTON project. A.K. S.S., and B.V.

acknowledge support from the Belgian federal government through the Energy Transition Fund for the T-REX project. Dr. Huguette Penxten is acknowledged for assistance in the FTIR measurements. J.E.D. is grateful to the Consejo Nacional de Investigaciones Científicas y Técnicas (CONICET) of Argentina for financial support. D.R.S acknowledges funds from the Fonds voor Wetenschappelijk Onderzoek – Vlaanderen (FWO) for the Ph.D. fellowship (No. 11PJZ24N). AS acknowledge CeSAR—Centro Servizi di Ateneo per la Ricerca at Università degli Studi di Cagliari and thank Dr. Riccardo Pau for assistance in laser spectroscopy measurements. A.S. was supported by PON R&I "Ricerca e Innovazione" 2014–2020 CCI2014IT16M2OP005 Azione IV.4. Contratti di ricerca su tematiche Green-CUP F35F210023900.

Author Contributions

A.K. and S.S. conceived the original idea. A.K. synthesized and characterized the samples. T.C. and A.V. performed the photoelectron spectroscopy measurements and analysis. L.A., J.D., A.K., and S.G. performed and analyzed photoelectrochemical and product quantification analysis. D.S., A.K., J.H., V.J., and L.L. performed structural and chemical characterization. A.K., S.S., L.A., J.D., A.V., G.B., and S.G. performed the formal data analysis. A.S. performed the photoluminescence analysis. A.K. wrote the original manuscript draft. S.S., L.A. J.D., V.J., S.G., G.B., and contributed to the discussion, revision, and completion of the manuscript. S.S., G.B., and B.V. supervised the work. All authors contributed to the scientific discussion and revision of the manuscript.

Notes

The authors declare no competing financial interests.

References

(1) Wang, X.; Maeda, K.; Thomas, A.; Takanabe, K.; Xin, G.; Carlsson, J. M.; Domen, K.; Antonietti, M. A metal-free polymeric photocatalyst for hydrogen production from water under visible light. *Nature materials* **2009**, *8* (1), 76-80.
(2) Volokh, M.; Peng, G.; Barrio, J.; Shalom, M. Carbon nitride materials for water splitting photoelectrochemical cells. *Angewandte Chemie International Edition* **2019**, *58* (19), 6138-6151.
(3) Koutavarapu, R.; Peera, S. G.; Lee, T. G.; Myla, C. R.; Lee, D.-Y.; Shim, J.; Balasingam, S. K. Recent trends in graphitic carbon nitride-based binary and ternary heterostructured electrodes for photoelectrochemical water splitting. *Processes* **2021**, *9* (11), 1959.
(4) He, B.; Cao, Y.; Lin, K.; Wang, Y.; Li, Z.; Yang, Y.; Zhao, Y.; Liu, X. Strong Interactions between Au Nanoparticles and BiVO4 Photoanode Boosts Hole Extraction for Photoelectrochemical Water Splitting. *Angewandte Chemie International Edition* **2024**, e202402435.
(5) Xia, M.; Zhao, X.; Lin, C.; Pan, W.; Zhang, Y.; Guo, Z.; Leung, D. Y. C. High-Voltage Etching-Induced Terrace-like WO3 Photoanode for Efficient Photoelectrochemical Water Splitting. *ACS Applied Energy Materials* **2023**, *6* (17), 8717-8728. DOI: 10.1021/acsaem.3c01164.
(6) Dong, Z.; Chen, M.; Qin, D.; Han, S. Recent advances and perspective of modified TiO2-based photoanodes toward photoelectrochemical water splitting. *Fuel* **2024**, *373*, 132366.
(7) He, Y.; Zhu, L.; Hu, J.; Zhang, Y.; Wang, J.; Zhang, C.; Li, J.; Leung, M. K.; Li, H. Enhanced photoelectrochemical activity of bi-functional photocatalytic fuel cell by a superior heterostructure SnO2/BiOBr/MoS2 photoanode. *Applied Surface Science* **2023**, *622*, 156821.
(8) Ji, M.-H.; Chen, Y.-X.; Chen, R.; Li, K.-X.; Zhao, H.-P.; Shi, H.-Y.; Wang, H.-L.; Jiang, X.; Lu, C.-Z. A novel α-Fe2O3 photoanode with multilayered In2O3/Co–Mn nanostructure for efficient photoelectrochemical water splitting. *International Journal of Hydrogen Energy* **2024**, *51*, 66-77.
(9) Wang, L.; Si, W.; Tong, Y.; Hou, F.; Pergolesi, D.; Hou, J.; Lippert, T.; Dou, S. X.; Liang, J. Graphitic carbon nitride (g‐C3N4)‐based nanosized heteroarrays: promising materials for photoelectrochemical water splitting. *Carbon Energy* **2020**, *2* (2), 223-250.
(10) Bian, J.; Li, Q.; Huang, C.; Li, J.; Guo, Y.; Zaw, M.; Zhang, R.-Q. Thermal vapor condensation of uniform graphitic carbon nitride films with remarkable photocurrent density for photoelectrochemical applications. *Nano Energy* **2015**, *15*, 353-361.
(11) Bian, J.; Li, J.; Kalytchuk, S.; Wang, Y.; Li, Q.; Lau, T. C.; Niehaus, T. A.; Rogach, A. L.; Zhang, R. Q. Efficient emission facilitated by multiple energy level transitions in uniform graphitic carbon nitride films deposited by thermal vapor condensation. *ChemPhysChem* **2015**, *16* (5), 954-959.
(12) Oo, M. T.; Tian, H.; Zhao, Y.; Zhang, R.-Q. Rapid thermal vapor condensation towards crystalline carbon nitride film with improved photoelectrochemical activity. *Journal of Physics D: Applied Physics* **2022**, *55* (44), 444001.
(13) Fan, X.; Wang, T.; Gao, B.; Xie, X.; Zhang, S.; Meng, X.; Gong, H.; Guo, Y.; Huang, X.; He, J. Layered double hydroxides decorated graphic carbon nitride film as efficient photoanodes for photoelectrochemical water splitting. *Catalysis Today* **2019**, *335*, 423-428.
(14) Xie, X.; Fan, X.; Huang, X.; Wang, T.; He, J. In situ growth of graphitic carbon nitride films on transparent conducting substrates via a solvothermal route for photoelectrochemical performance. *RSC advances* **2016**, *6* (12), 9916-9922.

(15) Mohamed, N. A.; Safaei, J.; Ismail, A. F.; Jailani, M. F. A. M.; Khalid, M. N.; Noh, M. F. M.; Aadenan, A.; Nasir, S. N. S.; Sagu, J. S.; Teridi, M. A. M. The influences of post-annealing temperatures on fabrication graphitic carbon nitride,(g-C3N4) thin film. *Applied Surface Science* **2019**, *489*, 92-100.
(16) Mohamed, N. A.; Safaei, J.; Ismail, A. F.; Noh, M. F. M.; Arzaee, N. A.; Mansor, N. N.; Ibrahim, M. A.; Ludin, N. A.; Sagu, J. S.; Teridi, M. A. M. Fabrication of exfoliated graphitic carbon nitride,(g-C3N4) thin film by methanolic dispersion. *Journal of Alloys and Compounds* **2020**, *818*, 152916.
(17) Ragupathi, V.; Panigrahi, P.; Subramaniam, N. G. Scalable fabrication of graphitic-carbon nitride thin film for optoelectronic application. *Materials Today: Proceedings* **2023**, *80*, 2115-2118.
(18) Peng, G.; Xing, L.; Barrio, J.; Volokh, M.; Shalom, M. A general synthesis of porous carbon nitride films with tunable surface area and photophysical properties. *Angewandte Chemie International Edition* **2018**, *57* (5), 1186-1192.
(19) Liu, J.; Wang, H.; Chen, Z. P.; Moehwald, H.; Fiechter, S.; van de Krol, R.; Wen, L.; Jiang, L.; Antonietti, M. Microcontact-printing-assisted access of graphitic carbon nitride films with favorable textures toward photoelectrochemical application. *Adv. Mater* **2015**, *27* (4), 712-718.
(20) Qin, J.; Barrio, J.; Peng, G.; Tzadikov, J.; Abisdris, L.; Volokh, M.; Shalom, M. Direct growth of uniform carbon nitride layers with extended optical absorption towards efficient water-splitting photoanodes. *Nature Communications* **2020**, *11* (1), 4701. DOI: 10.1038/s41467-020-18535-0.
(21) Adler, C.; Krivtsov, I.; Mitoraj, D.; dos Santos‐Gómez, L.; García‐Granda, S.; Neumann, C.; Kund, J.; Kranz, C.; Mizaikoff, B.; Turchanin, A. Sol− gel processing of water‐soluble carbon nitride enables high‐performance photoanodes. *ChemSusChem* **2021**, *14* (10), 2170-2179.
(22) Giusto, P.; Cruz, D.; Heil, T.; Arazoe, H.; Lova, P.; Aida, T.; Comoretto, D.; Patrini, M.; Antonietti, M. Shine bright like a diamond: new light on an old polymeric semiconductor. *Advanced Materials* **2020**, *32* (10), 1908140.
(23) Peng, G.; Albero, J.; Garcia, H.; Shalom, M. A water‐splitting carbon nitride photoelectrochemical cell with efficient charge separation and remarkably low onset potential. *Angewandte Chemie International Edition* **2018**, *57* (48), 15807-15811.
(24) Shmila, T.; Mondal, S.; Barzilai, S.; Karjule, N.; Volokh, M.; Shalom, M. Boron and Sodium Doping of Polymeric Carbon Nitride Photoanodes for Photoelectrochemical Water Splitting. *Small* **2023**, *19* (42), 2303602.
(25) Zhang, J.; Zhu, Y.; Njel, C.; Liu, Y.; Dallabernardina, P.; Stevens, M. M.; Seeberger, P. H.; Savateev, O.; Loeffler, F. F. Metal-free photoanodes for C–H functionalization. *Nature Communications* **2023**, *14* (1), 7104.
(26) Abisdris, L.; Tzadikov, J.; Karjule, N.; Azoulay, A.; Volokh, M.; Shalom, M. Electrophoretic deposition of supramolecular complexes for the formation of carbon nitride films. *Sustainable Energy & Fuels* **2020**, *4* (8), 3879-3883.
(27) Fang, Y.; Li, X.; Wang, X. Synthesis of polymeric carbon nitride films with adhesive interfaces for solar water splitting devices. *ACS Catalysis* **2018**, *8* (9), 8774-8780.
(28) Raub, A. A. M.; Bahru, R.; Nashruddin, S. N. A. M.; Yunas, J. Advances of nanostructured metal oxide as photoanode in photoelectrochemical (PEC) water splitting application. *Heliyon* **2024**.
(29) Zhang, B.; Yu, S.; Dai, Y.; Huang, X.; Chou, L.; Lu, G.; Dong, G.; Bi, Y. Nitrogen-incorporation activates NiFeOx catalysts for efficiently boosting oxygen evolution activity and stability of BiVO4 photoanodes. *Nature Communications* **2021**, *12* (1), 6969.

(30) Li, H.-J.; Qian, D.-J.; Chen, M. Templateless Infrared Heating Process for Fabricating Carbon Nitride Nanorods with Efficient Photocatalytic H2 Evolution. *ACS Applied Materials & Interfaces* **2015**, *7* (45), 25162-25170. DOI: 10.1021/acsami.5b06627.
(31) Jiang, T.; Wang, Z.; Wei, G.; Wu, S.; Huang, L.; Li, D.; Ruan, X.; Liu, Y.; Jiang, C.; Ren, F. Defective High-Crystallinity g-C3N4 Heterostructures by Double-End Modulation for Photocatalysis. *ACS Energy Letters* **2024**, *9* (4), 1915-1922.
(32) Katsina, A. U.; Cursaru, D.-L.; Matei, D.; Mihai, S. Effect of Morphology Modification of BiFeO3 on Photocatalytic Efficacy of Pg-C3N4/BiFeO3 Composites. *International Journal of Molecular Sciences* **2024**, *25* (9), 4948.
(33) Ma, Z.; Zhou, P.; Zhang, L.; Zhong, Y.; Sui, X.; Wang, B.; Ma, Y.; Feng, X.; Xu, H.; Mao, Z. A recyclable 3D gC 3 N 4 based nanocellulose aerogel composite for photodegradation of organic pollutants. *Cellulose* **2021**, *28*, 3531-3547.
(34) Dong, F.; Li, Y.; Wang, Z.; Ho, W.-K. Enhanced visible light photocatalytic activity and oxidation ability of porous graphene-like g-C3N4 nanosheets via thermal exfoliation. *Applied Surface Science* **2015**, *358*, 393-403.
(35) Katsumata, H.; Higashi, F.; Kobayashi, Y.; Tateishi, I.; Furukawa, M.; Kaneco, S. Dual-defect-modified graphitic carbon nitride with boosted photocatalytic activity under visible light. *Scientific reports* **2019**, *9* (1), 14873.
(36) He, X.; Wu, Z.; Xue, Y.; Gao, Z.; Yang, X. Fabrication of interlayer β-CD/gC 3 N 4@ MoS 2 for highly enhanced photodegradation of glyphosate under simulated sunlight irradiation. *RSC advances* **2019**, *9* (8), 4635-4643.
(37) Xing, W.; Li, C.; Chen, G.; Han, Z.; Zhou, Y.; Hu, Y.; Meng, Q. Incorporating a novel metal-free interlayer into g-C3N4 framework for efficiency enhanced photocatalytic H2 evolution activity. *Applied Catalysis B: Environmental* **2017**, *203*, 65-71.
(38) Zhang, J.-W.; Gong, S.; Mahmood, N.; Pan, L.; Zhang, X.; Zou, J.-J. Oxygen-doped nanoporous carbon nitride via water-based homogeneous supramolecular assembly for photocatalytic hydrogen evolution. *Applied Catalysis B: Environmental* **2018**, *221*, 9-16.
(39) Wu, J.; Liu, Z.; Lin, X.; Jiang, E.; Zhang, S.; Huo, P.; Yan, Y.; Zhou, P.; Yan, Y. Breaking through water-splitting bottlenecks over carbon nitride with fluorination. *Nature Communications* **2022**, *13* (1), 6999.
(40) Xiong, T.; Cen, W.; Zhang, Y.; Dong, F. Bridging the g-C3N4 Interlayers for Enhanced Photocatalysis. *ACS Catalysis* **2016**, *6* (4), 2462-2472. DOI: 10.1021/acscatal.5b02922.
(41) Dementjev, A.; De Graaf, A.; Van de Sanden, M.; Maslakov, K.; Naumkin, A.; Serov, A. X-Ray photoelectron spectroscopy reference data for identification of the C3N4 phase in carbon–nitrogen films. *Diamond and related materials* **2000**, *9* (11), 1904-1907.
(42) Barrio, J.; Lin, L.; Amo‐Ochoa, P.; Tzadikov, J.; Peng, G.; Sun, J.; Zamora, F.; Wang, X.; Shalom, M. Unprecedented Centimeter‐Long Carbon Nitride Needles: Synthesis, Characterization and Applications. *Small* **2018**, *14* (21), 1800633.
(43) Qin, J.; Wang, S.; Ren, H.; Hou, Y.; Wang, X. Photocatalytic reduction of CO2 by graphitic carbon nitride polymers derived from urea and barbituric acid. *Applied Catalysis B: Environmental* **2015**, *179*, 1-8.
(44) Zan, Z.; Li, X.; Gao, X.; Huang, J.; Luo, Y.; Han, L. 0D/2D carbon nitride quantum dots (CNQDs)/BiOBr S-scheme heterojunction for robust photocatalytic degradation and H2O2 production. *Acta Phys.-Chim. Sin.* **2023**, *39* (6), 2209016.
(45) Li, S.; Liu, W.; Zhao, S.; Li, Y.; Chen, K. Enhanced Photocatalytic Performance of NiS2/g‐C3N4/SnS2 by Improving the Charge Diffusion on Both Valence Band and Conduction Band of Carbon Nitride. *ChemistrySelect* **2021**, *6* (18), 4440-4447.
(46) Meng, L.; Zhou, X.; Wang, S.; Zhou, Y.; Tian, W.; Kidkhunthod, P.; Tunmee, S.; Tang, Y.; Long, R.; Xin, Y. A Plasma‐Triggered O− S Bond and P− N Junction Near the Surface of

a SnS2 Nanosheet Array to Enable Efficient Solar Water Oxidation. *Angewandte Chemie International Edition* **2019**, *58* (46), 16668-16675.
(47) Jin, T.; Liu, C.; Chen, F.; Qian, J.; Qiu, Y.; Meng, X.; Chen, Z. Synthesis of SnS2/Carbon Quantum Dots/g‐C3N4 Composite and Its Photocatalytic Property. *physica status solidi (a)* **2022**, *219* (22), 2200334.
(48) Jing, L.; Xu, Y.; Chen, Z.; He, M.; Xie, M.; Liu, J.; Xu, H.; Huang, S.; Li, H. Different morphologies of SnS2 supported on 2D g-C3N4 for excellent and stable visible light photocatalytic hydrogen generation. *ACS Sustainable Chemistry & Engineering* **2018**, *6* (4), 5132-5141.
(49) Zhang, Z.; Shao, C.; Li, X.; Wang, C.; Zhang, M.; Liu, Y. Electrospun nanofibers of p-type NiO/n-type ZnO heterojunctions with enhanced photocatalytic activity. *ACS applied materials & interfaces* **2010**, *2* (10), 2915-2923.
(50) Chen, W.; Qiu, Y.; Zhong, Y.; Wong, K. S.; Yang, S. High-efficiency dye-sensitized solar cells based on the composite photoanodes of SnO2 nanoparticles/ZnO nanotetrapods. *The Journal of Physical Chemistry A* **2010**, *114* (9), 3127-3138.
(51) Liang, Y.; Tsubota, T.; Mooij, L. P.; van de Krol, R. Highly improved quantum efficiencies for thin film BiVO4 photoanodes. *The Journal of Physical Chemistry C* **2011**, *115* (35), 17594-17598.
(52) Xiao, B.-C.; Lin, L.-Y.; Hong, J.-Y.; Lin, H.-S.; Song, Y.-T. Synthesis of a monoclinic BiVO 4 nanorod array as the photocatalyst for efficient photoelectrochemical water oxidation. *RSC advances* **2017**, *7* (13), 7547-7554.
(53) Mohd‐Nasir, S.; Mat‐Teridi, M.; Ebadi, M.; Sagu, J.; Sulaiman, M.; Ludin, N.; Ibrahim, M. Influence of ethylene glycol on efficient photoelectrochemical activity of BiVO4 photoanode via AACVD. *physica status solidi (a)* **2015**, *212* (12), 2910-2914.
(54) Zhang, G.; Xu, Y.; Rauf, M.; Zhu, J.; Li, Y.; He, C.; Ren, X.; Zhang, P.; Mi, H. Breaking the Limitation of Elevated Coulomb Interaction in Crystalline Carbon Nitride for Visible and Near‐Infrared Light Photoactivity. *Advanced Science* **2022**, *9* (21), 2201677.
(55) Wang, M.; Langer, M.; Altieri, R.; Crisci, M.; Osella, S.; Gatti, T. Two-dimensional layered heterojunctions for photoelectrocatalysis. *ACS nano* **2024**, *18* (13), 9245-9284.
(56) Yu, J.; Wang, Y.; Zhou, Y.; Fang, W.; Liu, B.; Xing, J. Intrinsic self-trapped excitons in graphitic carbon nitride. *Nano Letters* **2024**, *24* (15), 4439-4446.
(57) Karjule, N.; Barrio, J.; Xing, L.; Volokh, M.; Shalom, M. Highly efficient polymeric carbon nitride photoanode with excellent electron diffusion length and hole extraction properties. *Nano letters* **2020**, *20* (6), 4618-4624.